Original Article

http://dx.doi.org/10.3348/kjr.2011.12.5.602
pISSN 1229-6929 · eISSN 2005-8330
Korean J Radiol 2011;12(5):602-610

Korean Journal of Radiology
KJR

Evaluation of Antiangiogenic Effects of a New Synthetic Candidate Drug KR-31831 on Xenografted Ovarian Carcinoma Using Dynamic Contrast Enhanced MRI

Jehoon Yang, PhD[1], Jae-Hun Kim, PhD[1], Geun-Ho Im, MS[2], Hyejung Heo, MS[2], Sera Yoon, BSc[2], Jaewon Lee, MS[2], Jung Hee Lee, PhD[1], Pyoung Jeon, MD[1]

[1]Department of Radiology, Samsung Medical Center, Sungkyunkwan University School of Medicine, Seoul 135-710, Korea; [2]Center for Molecular and Cellular Imaging, Samsung Biomedical Research Institute, Samsung Medical Center, Seoul 135-710, Korea

Objective: The purpose of this research was to investigate the anti-angiogenic inhibitory effect of KR-31831, a newly developed anti-angiogenic agent, on an *in vivo* human ovarian carcinoma model using dynamic contrast-enhanced (DCE) MRI.
Materials and Methods: Xenografted ovarian tumors were established by subcutaneous injection of SKOV3 cells into mice. The mice were treated daily with KR-31831 at 50 mg/kg for 21 days. Tumor tissues were excised corresponding to the DCE-MRI sections for evaluation of MVD with CD31 immunohistochemistry. All *in vivo* MRIs were performed on a 7.0 Tesla micro-MRI System. DCE-MRI was acquired prior to initiating treatment with KR-31831 and again on days 3 and 21 after treatment. The permeability parameters (K^{trans}, v_e, and v_p) were estimated using a pharmacokinetic model.
Results: Qualitatively, the K^{trans} parametric mapping showed different changes before and after treatment with KR-31831 in the treatment group. For quantification of this change, the median of K^{trans} values were compared before and after treatments in the control and KR-31831-treated groups. A non-parametric statistical test (Wilcoxon signed-rank test) showed decreasing K^{trans} values on day 21 compared to days 0 and 3 in the KR-31831-treated group ($p < 0.05$), whereas there was no significant difference in the control group ($p = 0.84$).
Conclusion: Our results suggest that DCE-MRI can be a useful tool by which to evaluate the anti-angiogenic effect of KR-31831 on a xenografted human ovarian carcinoma model.

Index terms: *Angiogenesis; Dynamic contrast-enhanced MRI; Microvascular density; KR-31831; VEGF*

INTRODUCTION

Angiogenesis is the process by which new blood vessels develop from existing microvasculature in a variety of physiologic states. Angiogenesis is essential for solid tumor growth, invasion and metastatic pathway. Without angiogenesis, tumor growth cannot proceed beyond 1-2 mm^2 because tumor growth is severely limited by oxygen, the nutrient supply, and removal of waste products into the surrounding medium (1-3). For many tumors, vascular density provides a prognostic indicator of metastatic potential, with highly vascular primary tumors having a higher incidence of metastasis than poorly vascular tumors. Tumor angiogenesis is a promising targeting for development of novel anti-cancer therapies because endothelial cells are thought to be genetically stable compared with tumor cells.

Tumor angiogenesis is regulated by the production of angiogenic stimulators and inhibitors. In recent years, it has been well-established that tyrosine kinase receptors

Received October 6, 2010; accepted after revision April 12, 2011.
Corresponding author: Pyoung Jeon, MD, Department of Radiology, Samsung Medical Center, Sungkyunkwan University School of Medicine, 50 Ilwon-dong, Gangnam-gu, Seoul 135-710, Korea.
• Tel: (822) 3410-6433 • Fax: (822) 3410-3628
• E-mail: drpjeon@gmail.com

Korean Journal of Radiology
KJR

of vascular endothelial growth factor (VEGF), fibroblast growth factor (FGF), and platelet-derived growth factor (PDGF) are strongly implicated in angiogenesis associated with solid tumors (4-8). One of the most specific and critical regulators of angiogenesis is VEGF, which regulates endothelial proliferation, permeability, and survival. VEGF is a mitogen for vascular endothelial cells derived from arteries, veins, and lymphatics (6, 9). VEGF has been shown to play a coordinated role in endothelial cell proliferation and assembly of the vessel wall in a variety of normal and abnormal circumstances by activating the mitogen-activated protein kinase/extracellular signal-regulated kinase and phosphatidylinositol 3'-kinase/AKT pathways, and VEGF is also a survival factor for normal and tumor endothelium (5, 10). The VEGF signaling pathway is activated by ligand-induced phosphorylation of the VEGF receptors (VEGFRs). The blocking of VEGFR phosphorylation by a kinase inhibitor is expected to disrupt VEGF signaling pathways resulting in changes in tumor vascular characteristics and growth (10-13).

(2R,3R,4S)-6-amino-4-[n-(4-chlorophenyl)-N-(1H-imidazon-2ylmethyl)amino]-3-hydroxyl-2-methyl-2dimenhoxymethyl-3,4-dihydro-2H-1-benzopran (KR-31831) is a newly developed small molecular weight drug used as an anti-angiogenic inhibitor in our co-worker group. KR-31831 has been reported to suppress endothelial cell proliferation, tube formation, invasion, and migration *in vitro* (14, 15, 17). Also, KR-31831 inhibits vessel formation in the mouse Matrigel plug assay *in vivo* (15-17). Although the specific mechanisms underlying the anti-angiogenic effects of this new synthetic agent are not fully understood, the inhibitory mechanism of KR-31831 on tumor angiogenesis, especially on the VEGF-signaling pathway in human umbilical vein endothelial cells (HUVECs), has been thoroughly studied. KR-31831 down-regulates VEGF-induced tumor formation and proliferation of HUVECs by inhibiting intracellular Ca^{2+} release and phosphorylation of extracellular regulated kinase 1/2 (Erk1/2). Moreover, the expression of VEGF receptor 2 (VEGFR2 [also known as Flk-1 or KDR]) was also reduced by the treatment of KR-31831 (16, 17).

Technical advances in magnetic resonance imaging (MRI) have improved the non-invasive measurement of functional information about tumors for the diagnosis and assessment of treatment response (18, 19). Dynamic contrast-enhanced (DCE) MRI has the ability to non-invasively detect morphologic and functional characteristics of tumor vasculature, including the anti-angiogenic response of tumors by the differential distribution of contrast agent in tissues (20). By quantification of tumor perfusion and capillary permeability, this technique allows for assessment of anti-angiogenic treatment response more readily than indirect and delayed assessment of tumor size.

In the current study we tested the *in vivo* anti-angiogenic efficacy of the newly developed angiogenesis inhibitor, KR-31831, using quantification of DCE-MRI in mice bearing SKOV3 tumor.

MATERIALS AND METHODS

Cell Culture

The human ovarian carcinoma cell line, SKOV3, was obtained from the American Type Culture Collection (Manassas, VA) and cultured in RPMI-1640 medium supplemented with 10% fetal bovine serum (FBS) and 1% ampicillin and streptomycin. Cells were cultured at 37°C in a humidified incubator containing 5% CO_2 and routinely passaged twice a week at a split ratio of 1:3. All experiments were performed with 70-80% confluent cultures.

Subcutaneous Ectopic Xenograft Tumor Model and Treatment

The anti-angiogenic efficacy of KR-31831 was tested in mice bearing ectopic SKOV3 tumors. Female BALB/c nu/nu mice (7 weeks old) were purchased from Orient Bio (Seoul, South Korea) and housed in specific pathogen-free conditions. The mice were cared for in accordance with guidelines set forth by the American Association for the Accreditation of Laboratory Animal Care (AAALAC), and all studies with mice were reviewed and approved by the Institutional Animal Care and Use Committee (IACUC) of Samsung Biomedical Research Institute (SBRI). SBRI is an Association for Assessment and Accreditation of Laboratory Animal Care International-accredited facility and abides by the Institute of Laboratory Animal Resources (ILAR) guide. Ectopic xenograft tumors were established by subcutaneous injection of 2×10^6 SKOV3 cells in a total volume of 0.1 mL of a serum-free medium containing 50% Matrigel (BD Bioscience, Erembodegem, Belgium) into the right thigh under isoflurane anesthesia. As the tumors became palpable, the mice were randomly assigned into treatment and control groups (six mice per group). KR-31831 was obtained from the Korea Research Institute of Chemical Technology and prepared as a suspension in vehicle (10% cremophor [vol/

vol] and 10% absolute ethyl alcohol [vol/vol] in normal saline) for intraperitoneal injection into xenograft-bearing athymic nude mice. KR-31831 therapy was initiated 14 days after THE cell line injection. In the treated group (n = 6), mice were treated daily with KR-31831 (50 mg/kg). In the control group (n = 6), mice were also treated daily with vehicle alone intraperitoneally for 21 days. Immediately after DCE-MRI data acquisition, all of the mice were maintained under anesthesia using 1.5% isoflurane, 70% N_2O, and 30% O_2, and transcardially perfused with 0.9% normal saline followed by 10% neutral buffered formalin (NBF) solution. For the subsequent histologic analysis, the tumor tissue was removed, fixed further in 10% NBF for 24 hrs, then sliced in accordance with MR images.

MRI Data Acquisition

All data were obtained using a 7.0 Tesla (T) micro-MRI System (20 cm gradient set, and 72 mm i.d. birdcage coil; Bruker-Biospin, Fallanden, Switzerland). Mice were anesthetized with 1.5% isoflurane in 70% N_2O and 30% O_2 using an MR-compatible mobile inhalation anesthesia system. DCE-MR imaging was performed using a coronal T_1-weighted 3D gradient echo sequence, as follows: FLASH sequence; TR = 67 ms; TE = 3 ms; flip angle = 70°; FOV = 30 x 30 mm; imaging matrix = 128 x 128; slice thickness = 2.5 mm; temporal resolution = 6 s; and 120 dynamics. For T_1 mapping, 5 pre-contrast scans were acquired with the same post-contrast parameters, but different flip angles (5°, 15°, 35°, 60°, and 70°). Baseline images were acquired for approximately 60 s, followed by an automatic injection over 4-5 s of 0.1 mmol/kg of Dotarem via the tail vein, followed by further acquisitions, up to a total time of 12 min (120 images).

MRI Data Analysis

The concentration of contrast agent was estimated by determination of the difference in longitudinal relaxation rates, as follows: $C(t) = (1/T_1[t] - 1/T_1[0])/r1$, where T_1 (t) and T_1 (0) are the post- and pre-contrast T_1 values, respectively, and r1 denotes the longitudinal relaxivity (2.92 $s^{-1}mM^{-1}$; 20). DCE-MRI data were converted into the concentration of the contrast agent using a different flip angle method (21). The general equation for SI values at a given flip angle is as follows:

$$SI(\alpha) = \frac{M_0\left(1 - e^{-\frac{TR}{T1}}\right)\sin\alpha}{\left(1 - \cos\alpha e^{-\frac{TR}{T1}}\right)}$$

where TR is the repetition time, α is the flip angle, and M_0 is the equilibrium longitudinal magnetization. The M_0 and T_1 parameter were estimated by a linear least-squares method using 5 MR images (5°, 15°, 35°, 60°, and 70°). Following the estimation of M_0 and T_1 (0) values for the pre-contrast image, post-contrast T_1 value (T_1 [t]) can be estimated as a function of time from the SI (t) for the post-contrast image with an α = 70°.

We used the extended Kety two-compartment model for quantification of tissue concentration (22), as follows:

$$C_t(t) = K^{trans} C_p(t) \otimes \exp\left(\frac{-K^{trans}}{v_e}\right) + v_p C_p(t) \quad (18)$$

where C_t is the concentration of the contrast agent in the observed tissue, C_P is the concentration in blood plasma, v_p is the fractional blood plasma volume per unit volume of tissue, K^{trans} is the volume transfer constant, and v_e is the fractional extravascular extracellular space (EES) per unit volume of tissue. The homemade software was implemented for performance of non-linear fitting of tissue concentration curves using the MATLAB *lsqnonlin* function.

The arterial input function (AIF) was manually defined at baseline for each mouse using Analysis of Functional NeuroImages (AFNI [http://afni.nimh.nih.gov/afni/)] (23), and used for quantification of DCE-MRI on days 0, 3, and 21. With AFNI software, users move the cursor to the voxel in a concentration image window; the corresponding concentration time curve is then displayed in a time profile window. The AIF voxels were manually selected in a voxel-by-voxel manner by visual inspection of voxel concentration profiles in AFNI software.

Immunohistochemical Analysis for Quantification of Microvessel Density

Formalin-fixed, paraffin-embedded tumor tissues were serially sliced into 5 μm sections corresponding to the magnetic resonance images for quantification of microvessel density (MVD) with CD31 staining by the immunohistochemical method. After heat-induced antigen retrieval for 20 min in citrate buffer (pH 6.0), endogenous peroxidase was blocked with 3% hydrogen peroxide in phosphate-buffered saline (PBS) for 10 min. Non-specific epitopes were blocked with blocking solution (2.5% normal

Korean Journal of Radiology
KJR

horse serum) for 20 min at room temperature followed by incubation with anti-mouse CD31 (1:150; BD-Pharmingen, Erembodegem, Belgium) antibody diluted in PBS containing 1% bovine serum albumin at room temperature for 30 min. After washing with PBS, the tissue sections were incubated with biotin-conjugated IgG for 30 min, then washed again followed by incubation with horseradish peroxidase (HRP)-conjugated streptavidin for 30 min. The color reaction was developed using the chromogen 3,3-diaminobenzidine (DAB) for 5 min. After washing, the tissue sections were lightly counterstained with Mayer's hematoxylin before dehydration and mounting. MVD was determined by examining the viable tumor area without necrosis in 12 mice (control [n = 6] and treated [n = 6]), as described previously (24). Individual microvessels were counted in 5 random fields per individual tumor section at 200X magnification. Brown-staining endothelial cells that were clearly separate in brown appearance were counted as individual vessels. The results were expressed as an average of the total number of microvessels observed in each individual tumor.

Statistical Analysis

The pharmacokinetic parameters (K^{trans}, v_e, and v_p) were estimated from DCE-MRI data using the pharmacokinetic modeling method before and after treatment with KR-31831 (3 and 21 days). The median and range of pharmacokinetic parameters were examined. The non-parametric statistical analysis (Wilcoxon signed-rank test) was performed to test significant differences in pharmacokinetic parameters before and after treatment with KR-31831 at a $p < 0.05$.

RESULTS

The AIF was manually defined by visual inspection of concentration profiles before treatment (day 0). Figure 1A shows representative images of the AIF near the femoral artery, and Figure 1B demonstrates the concentration profile of the AIF, which was averaged across the manually-defined AIF voxels in Figure 1A.

For quantification of DCE-MRI parameters, the regions of interest (ROI) were manually-defined on anatomic T2-weighted images, as shown in Figure 2A. A non-linear fitting method was used to fit the observed concentration profiles of tumor tissues (C_t) and arterial vessels (C_p) into the pharmacokinetic model (the extended Kety two-compartment model). The fitted concentration of tumor tissues is shown in Figure 2B; the results showed that the estimated K^{trans} parameter was 0.145, the v_e was 0.868, and the v_p was 0.0441.

Figure 3 shows the representative pharmacokinetic parametric mapping obtained from the control mice (Fig. 3A) and the KR-31831-treated mice (Fig. 3B) on days 0, 3, and 21 after treatment. To quantify changes in parameters between before and after treatment, the medians of the pharmacokinetic parameters (K^{trans}, v_e, and v_p) were extracted from the tumor region for each subject, and these parameters were compared on days 0, 3, and 21 after treatment for each group (Table 1). Figure 4 demonstrated that there were significant decreasing K^{trans} values on day 21 compared to days 0 and 3 in the KR-31831-treated group ($p < 0.05$), whereas there was no significant difference in the control group ($p = 0.84$) using the Wilcoxon signed-rank test. There was no significant difference between the

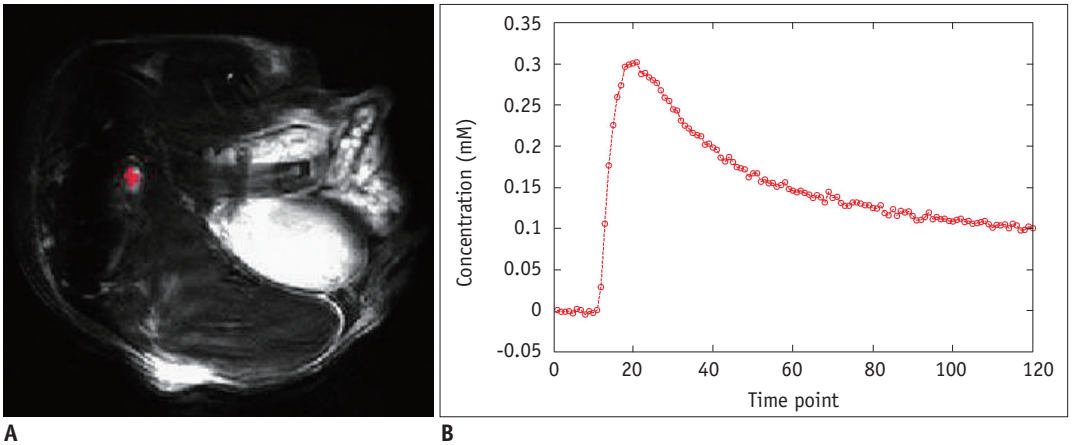

A B

Fig. 1. Determination of arterial input function.
A. Manually-defined arterial input function voxels by visual inspection of concentration time curves are shown in red. **B.** Representative concentration profile of arterial input function defined in **A**.

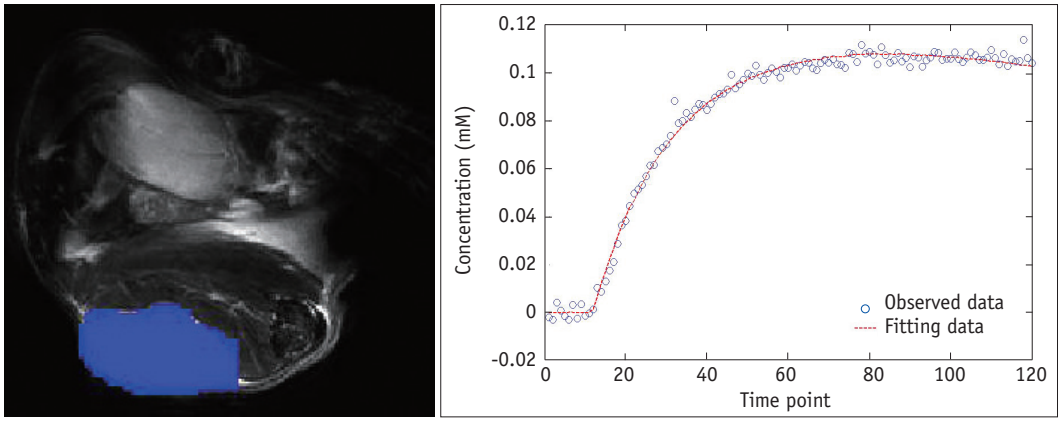

A B

Fig. 2. Non-linear fitting using pharmacokinetic modeling method.
A. Manually-defined tumor region is shown in blue. **B.** Representative concentration profile of tumor region (blue circle), and fitted data (red dot-line) using non-linear fitting method.

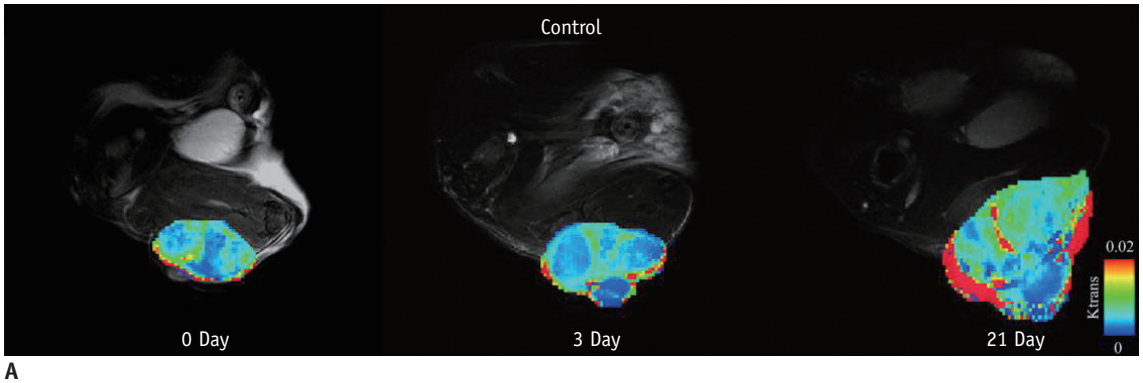

A

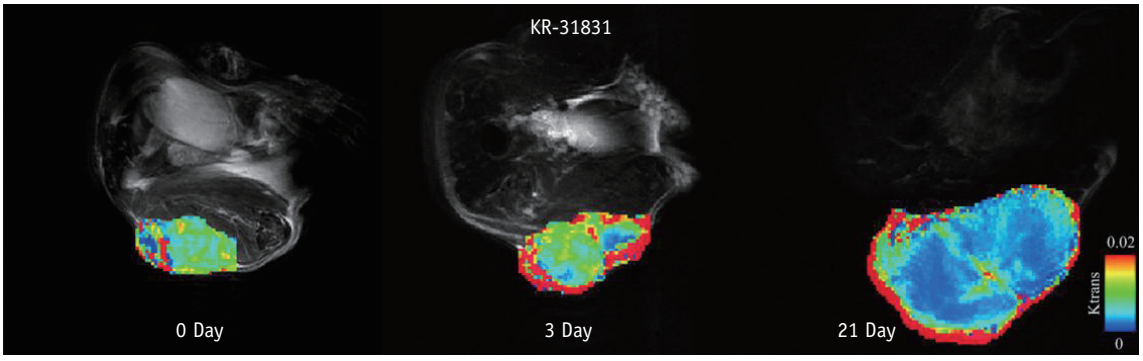

B

Fig. 3. Pharmacokinetic parametric mapping in control and KR-31831-treated mice on days 1, 3, and 21.
A. K^{trans} map for control mice. **B.** K^{trans} map for KR-31831-treated mice. Color schema ranges from 0 (blue) to 0.02 (red).

control and KR-31831 groups with respect to K^{trans} values at baseline (day 0); other parameters (v_e, and v_p) were not significantly different in the KR-31831-treated and control groups.

Immunohistochemical analysis for MVD performed on control and KR-31831-treated tumor tissues 21 days after treatment. As shown in Figure 5, tumor microvessels immunohistochemically analyzed with CD31 antibody reactivity in vascular tumor areas without necrosis in corresponding MRI sections were also significantly reduced in KR-31831-treated tumors compared to controls. Quantitative analysis of MVD was performed by examining individual microvessels in five random fields per tumor section under high-field magnification. The MVD was 18.6 ± 5.2 in control mice, while the MVD was 14.9 ± 4.0 and significantly reduced by approximately 20% in KR-31831-

Korean Journal of Radiology
KJR

Table 1. Descriptive Statistics of K^{trans}, v_e, and v_p Values on Days 0, 3, or 21 after Treatment in Each Group

	0 Day		3 Days		21 Days	
	Control	KR-31831	Control	KR-31831	Control	KR-31831
K^{trans}	0.008 (0.0061-0.0093)	0.0099 (0.0062-0.0194)	0.0099 (0.0044-0.0137)	0.0108 (0.0063-0.0146)	0.0043 (0.0031-0.0072)	0.0057 (0.0045-0.0069)
v_e	0.3137 (0.1959-0.5958)	0.3802 (0.3020-0.5559)	0.4022 (0.2297-0.6021)	0.432 (0.2788-0.6089)	0.3077 (0.1930-0.7080)	0.3296 (0.2908-0.3806)
v_p	0.015 (0.0028-0.0314)	0.0207 (0.0114-0.0527)	0.0286 (0.0117-0.0444)	0.0319 (0.0089-0.0582)	0.0246 (0.0071-0.0567)	0.0185 (0.0056-0.0374)

Note.— All data are presented as median and range (minimum and maximum).

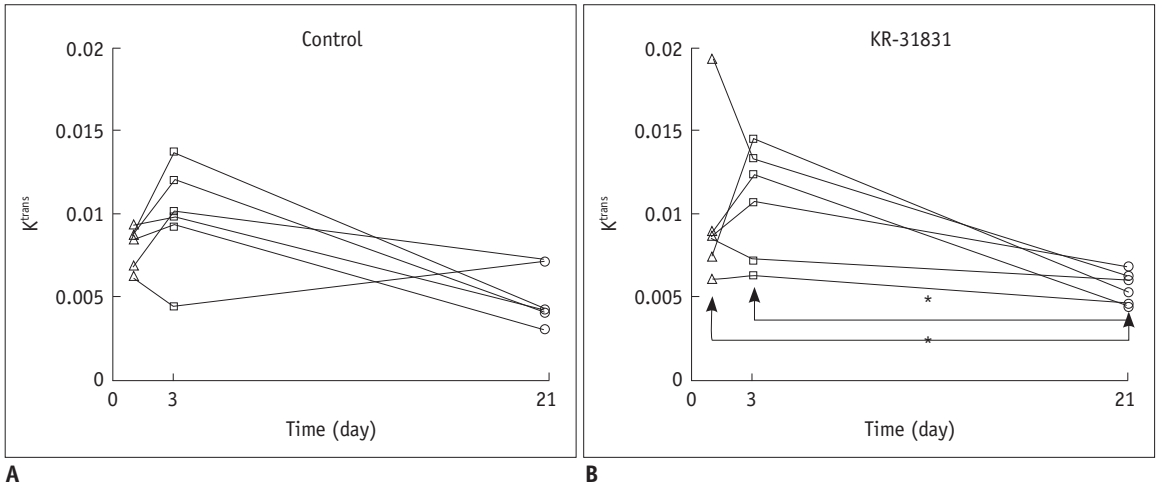

Fig. 4. Wilcoxon signed-rank test (K^{trans} parameter) before and after treatments in control and KR-31831-treated groups. *p < 0.05

treated mice (p < 0.05) (Fig. 5C).

DISCUSSION

Angiogenesis, the recruitment of new blood vessels, is the process by which new blood vessels grow in a variety of physiologic and pathophysiologic states. However, it is still a matter of debate whether or not MVD is a good indicator of the therapeutic efficacy of anti-angiogenic drugs. targeting angiogenesis represents a promising strategy for the development of anti-cancer drugs as several pre-clinical studies have shown that angiogenesis is a key pathway for tumor growth, invasion, and metastasis (3, 6, 10, 25). Furthermore, clinical trials in cancer patients are ongoing with several VEGF inhibitors, including a humanized monoclonal antibody (26) and various small molecules inhibiting signal transduction (9, 27, 28).

A number of endogenous proteins that act as positive regulators or activators of tumor angiogenesis have been identified, including VEGF, basic fibroblast growth factor (bFGF), tumor necrosis factor alpha (TNF-α), angiopoietin-1 and -2, interleukin (IL)-8, and platelet-derived growth factor beta (PDGF-ß; 10, 27). One of the more potent endothelial mitogens is VEGF, also known as vascular permeability factor (VPF) because it was initially recognized for its ability to increase microvascular permeability. VEGF is widely distributed and has been shown to play a coordinated role on the vascular endothelium, including endothelial mitogenesis, permeability, vascular tone, the production of vasoactive molecules, and the stimulation of monocyte chemotaxis (6, 13, 26). There are five members of the VEGF family in addition to four members of the angiopoietin family and at least one member of the ephrin family of regulators; the regulators must all work in a complementary and coordinated manner to form functional vessels (5, 25). A large number of anti-angiogenic drugs have been targeted against the angiogenic cytokine, VEGF. This cytokine is a principal mediator of vascular permeability, which has been measured by DCE-MRI and used as a pharmacodynamic end point for the development of these new compounds. Therefore, we designed this study to evaluate the anti-angiogenic efficacy of KR-31831 using DCE-MRI.

KR-31831 is a 4-(N-imidazol-2-ylmethyl) aminobenzopyran

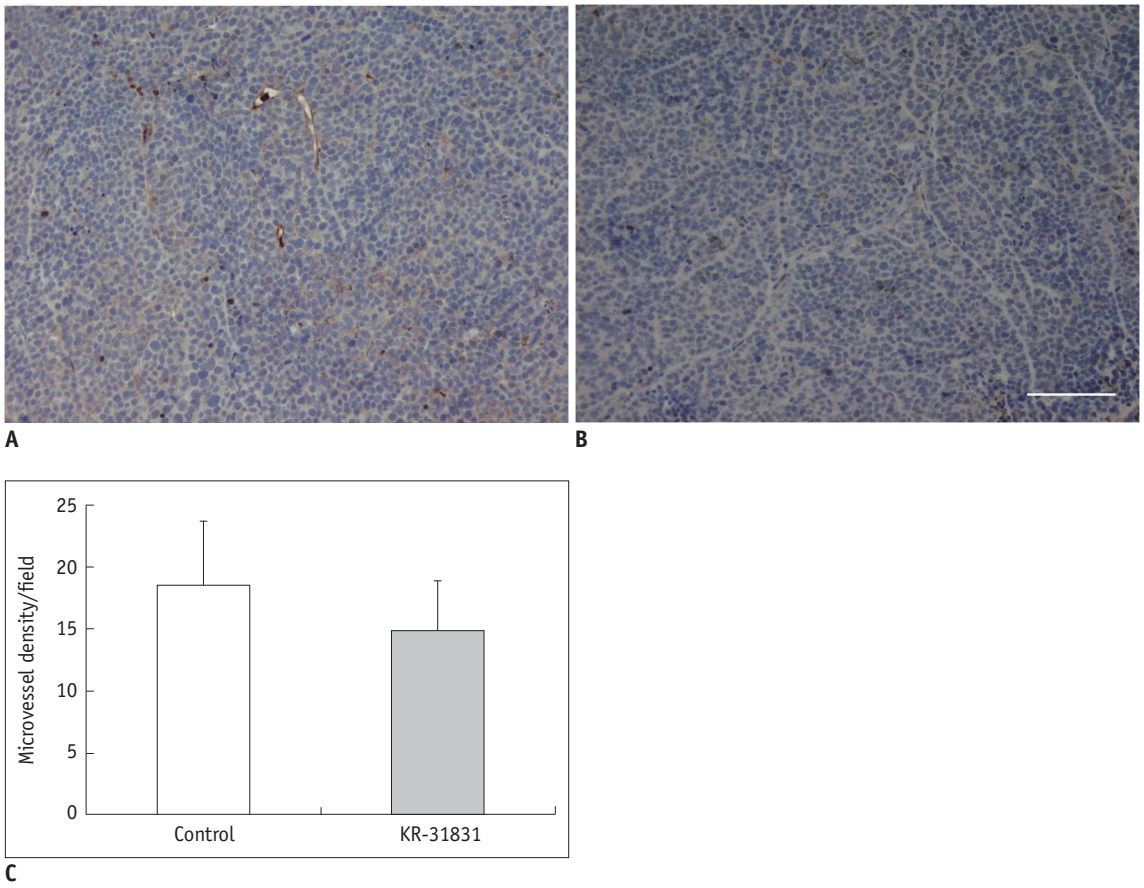

Fig. 5. Representative immunohistochemical analysis of microvessel density of xenografted SKOV3 tumor tissues obtained from control (A) and KR-31831-treated groups (B) in accordance with dynamic contrast-enhanced MRI sections at end time point of treatment. Vessels show dark brown color. Scale bar, 100 μm. Microvessel density was quantified and averaged in five random fields without necrosis per tumor at 200X magnification. Note microvessel density/field **(C)** was significantly reduced in tumor tissue from KR-31831 treatment group (14.9 ± 4.0) compared with control group (18.6 ± 5.2). $p < 0.05$. Error bars, SD.

analogue originally designed for the treatment of ischemic diseases, such as myocardial infarction and stroke, by a group of our co-workers (16, 17). Benzopran is one of the most frequently used backbones of synthetic drugs, including anti-oxidants, anti-hypertensives, and therapeutic agents for ischemia-related diseases. A variety of amines were introduced at the 4-position of benzopyran for the identification of adenosine triphosphate (ATP)-sensitive potassium channel (K_{ATP}) openers targeting ischemic disease, such as myocardial infarction and stroke. Previously, the group of co-workers demonstrated the ability of KR-31831 to inhibit VEGF-induced vascular permeability in *in vitro* and *in vivo* experiments (14, 15). Specifically, KR-31831 was shown to exert anti-angiogenic activities as measured by the inhibitory effect on HUVEC tube formation. Additionally, KR-31831 also showed inhibitory effects on VEGF-activated cell proliferation, migration, and invasion.

Dynamic contrast-enhanced MRI involves the acquisition of sequential images during the passage of a contrast agent through a particular tissue of interest. Analysis of DCE-MR images allows the generation of signal intensity versus time graphs. There have been two kinds of methods for quantification of DCE-MRI. Semi-quantitative analysis is based on the characterization of shape of time-to-signal curves which enable measurement of maximum enhancement, peak enhancement, before arrival time, and wash-in and -out slopes (29-31). However, these parameters are not associated with physiologic parameters, and are also not comparable among different MRI scanners. Alternative methods have been developed based on the pharmacokinetic model to estimate physiologic parameters, which have been proposed by Tofts and Kermode (32), Brix et al. (33), and Larsson et al. (34). These different models have been standardized in terms of quantities and symbols based on the assumption that tissue is composed of the extravascular extracellular space (EES) and the plasma space (v_p), and the transport between EES and v_p (volume transfer constant, K^{trans}; 22). In the current study, we used

Korean Journal of Radiology
KJR

the generalized Tofts model (extended Kety model) to quantify pharmacokinetic parameters form murine data, and our results showed the feasibility of DCE-MRI tools for evaluation of anti-angiogenic efficacy of the newly developed angiogenesis inhibitor, KR-31831.

In conclusion, the effect of KR-31831 on xenografted human ovarian tumor vasculature has been studied using DEC-MRI and a CD31 immunohistochemical method. As expected, a significant reduction in MVD was in agreement with the DCE-MRI finding of a decrease in fractional plasma volume and transendothelial permeability, thus providing a very robust demonstration of KR-31831 efficacy. Our results indicate that KR-31831 may offer opportunities for novel therapeutic strategies in ovarian carcinoma and DCE-MRI may be a useful tool to evaluate the effect of newly developed candidate drugs (such as KR-31831) on angiogenesis.

REFERENCES

1. Folkman J. What is the evidence that tumors are angiogenesis dependent? *J Natl Cancer Inst* 1990;82:4-6
2. Boehm T, Folkman J, Browder T, O'Reilly MS. Antiangiogenic therapy of experimental cancer does not induce acquired drug resistance. *Nature* 1997;390:404-407
3. Ko EY, Lee SH, Kim HH, Kim SM, Shin MJ, Kim N, et al. Evaluation of tumor angiogenesis with a second-generation US contrast medium in a rat breast tumor model. *Korean J Radiol* 2008;9:243-249
4. Conn G, Bayne ML, Soderman DD, Kwok PW, Sullivan KA, Palisi TM, et al. Amino acid and cDNA sequences of a vascular endothelial cell mitogen that is homologous to platelet-derived growth factor. *Proc Natl Acad Sci U S A* 1990;87:2628-2632
5. Fox SB, Gasparini G, Harris AL. Angiogenesis: pathological, prognostic, and growth-factor pathways and their link to trial design and anticancer drugs. *Lancet Oncol* 2001;2:278-289
6. Ferrara N, Davis-Smyth T. The biology of vascular endothelial growth factor. *Endocr Rev* 1997;18:4-25
7. Ferrara N, Henzel WJ. Pituitary follicular cells secrete a novel heparin-binding growth factor specific for vascular endothelial cells. *Biochem Biophys Res Commun* 1989;161:851-858
8. Plouet J, Schilling J, Gospodarowicz D. Isolation and characterization of a newly identified endothelial cell mitogen produced by AtT-20 cells. *EMBO J* 1989;8:3801-3806
9. Wood JM, Bold G, Buchdunger E, Cozens R, Ferrari S, Frei J, et al. PTK787/ZK 222584, a novel and potent inhibitor of vascular endothelial growth factor receptor tyrosine kinases, impairs vascular endothelial growth factor-induced responses and tumor growth after oral administration. *Cancer Res* 2000;60:2178-2189
10. Dvorak HF, Brown LF, Detmar M, Dvorak AM. Vascular permeability factor/vascular endothelial growth factor, microvascular hyperpermeability, and angiogenesis. *Am J Pathol* 1995;146:1029-1039
11. Prewett M, Huber J, Li Y, Santiago A, O'Connor W, King K, et al. Antivascular endothelial growth factor receptor (fetal liver kinase 1) monoclonal antibody inhibits tumor angiogenesis and growth of several mouse and human tumors. *Cancer Res* 1999;59:5209-5218
12. Kozin SV, Boucher Y, Hicklin DJ, Bohlen P, Jain RK, Suit HD. Vascular endothelial growth factor receptor-2-blocking antibody potentiates radiation-induced long-term control of human tumor xenografts. *Cancer Res* 2001;61:39-44
13. Mesiano S, Ferrara N, Jaffe RB. Role of vascular endothelial growth factor in ovarian cancer: inhibition of ascites formation by immunoneutralization. *Am J Pathol* 1998;153:1249-1256
14. Park SY, Seo EH, Song HS, Jung SY, Lee YK, Yi KY, et al. KR-31831, benzopyran derivative, inhibits VEGF-induced angiogenesis of HUVECs through suppressing KDR expression. *Int J Oncol* 2008;32:1311-1315
15. Yi EY, Park SY, Song HS, Son MJ, Yi KY, Yoo SE, et al. KR-31831, a new synthetic anti-ischemic agent, inhibits in vivo and in vitro angiogenesis. *Exp Mol Med* 2006;38:502-508
16. Kim HH, Paek IB, Ji HY, Lee S, Yi KY, Lee HS. Metabolism of a novel antiangiogenic agent KR-31831 in rats using liquid chromatography-electrospray mass spectrometry. *J Sep Sci* 2005;28:1818-1822
17. Kim SJ, Lee HI, Ji HY, Moon Y, Paek IB, Lee S, et al. Pharmacokinetics of a novel antiangiogenic agent KR-31831 in rats. *Biopharm Drug Dispos* 2005;26:21-26
18. O'Connor JP, Jackson A, Parker GJ, Jayson GC. DCE-MRI biomarkers in the clinical evaluation of antiangiogenic and vascular disrupting agents. *Br J Cancer* 2007;96:189-195
19. Zahra MA, Hollingsworth KG, Sala E, Lomas DJ, Tan LT. Dynamic contrast-enhanced MRI as a predictor of tumour response to radiotherapy. *Lancet Oncol* 2007;8:63-74
20. Pedersen M, Morkenborg J, Jensen FT, Stodkilde-Jorgensen H, Djurhuus JC, Frokiaer J. In vivo measurements of relaxivities in the rat kidney cortex. *J Magn Reson Imaging* 2000;12:289-296
21. Deoni SC, Rutt BK, Peters TM. Rapid combined T1 and T2 mapping using gradient recalled acquisition in the steady state. *Magn Reson Med* 2003;49:515-526
22. Tofts PS, Brix G, Buckley DL, Evelhoch JL, Henderson E, Knopp MV, et al. Estimating kinetic parameters from dynamic contrast-enhanced T(1)-weighted MRI of a diffusable tracer: standardized quantities and symbols. *J Magn Reson Imaging* 1999;10:223-232
23. Cox RW. AFNI: software for analysis and visualization of functional magnetic resonance neuroimages. *Comput Biomed Res* 1996;29:162-173
24. Shinriki S, Jono H, Ota K, Ueda M, Kudo M, Ota T, et al. Humanized anti-interleukin-6 receptor antibody suppresses tumor angiogenesis and in vivo growth of human oral

squamous cell carcinoma. *Clin Cancer Res* 2009;15:5426-5434
25. Pandya NM, Dhalla NS, Santani DD. Angiogenesis--a new target for future therapy. *Vascul Pharmacol* 2006;44:265-274
26. Presta LG, Chen H, O'Connor SJ, Chisholm V, Meng YG, Krummen L, et al. Humanization of an anti-vascular endothelial growth factor monoclonal antibody for the therapy of solid tumors and other disorders. *Cancer Res* 1997;57:4593-4599
27. Strawn LM, McMahon G, App H, Schreck R, Kuchler WR, Longhi MP, et al. Flk-1 as a target for tumor growth inhibition. *Cancer Res* 1996;56:3540-3545
28. Jun HY, Yin HH, Kim SH, Park SH, Kim HS, Yoon KH. Visualization of tumor angiogenesis using MR imaging contrast agent Gd-DTPA-anti-VEGF receptor 2 antibody conjugate in a mouse tumor model. *Korean J Radiol* 2010;11:449-456
29. Xiong HQ, Herbst R, Faria SC, Scholz C, Davis D, Jackson EF, et al. A phase I surrogate endpoint study of SU6668 in patients with solid tumors. *Invest New Drugs* 2004;22:459-466
30. Thomassin-Naggara I, Bazot M, Darai E, Callard P, Thomassin J, Cuenod CA. Epithelial ovarian tumors: value of dynamic contrast-enhanced MR imaging and correlation with tumor angiogenesis. *Radiology* 2008;248:148-159
31. Hillman GG, Singh-Gupta V, Zhang H, Al-Bashir AK, Katkuri Y, Li M, et al. Dynamic contrast-enhanced magnetic resonance imaging of vascular changes induced by sunitinib in papillary renal cell carcinoma xenograft tumors. *Neoplasia* 2009;11:910-920
32. Tofts PS, Kermode AG. Measurement of the blood-brain barrier permeability and leakage space using dynamic MR imaging. 1. Fundamental concepts. *Magn Reson Med* 1991;17:357-367
33. Brix G, Semmler W, Port R, Schad LR, Layer G, Lorenz WJ. Pharmacokinetic parameters in CNS Gd-DTPA enhanced MR imaging. *J Comput Assist Tomogr* 1991;15:621-628
34. Larsson HB, Stubgaard M, Frederiksen JL, Jensen M, Henriksen O, Paulson OB. Quantitation of blood-brain barrier defect by magnetic resonance imaging and gadolinium-DTPA in patients with multiple sclerosis and brain tumors. *Magn Reson Med* 1990;16:117-131